Continuous distribution of thermodynamic microprocesses in complex metastable systems

K. Krištiaková and P. Švec
Institute of Physics, Slovak Academy of Sciences, Dúbravská cesta 9, 84228 Bratislava, Slovakia
(Received 21 May 2000; revised manuscript received 28 September 2000; published 19 October 2001)

An approach to the determination of the number and probability of the occurrence of processes active in transitions from metastable to a more stable thermodynamic state without postulating *a priori* the form of their distribution is described. This aim is achieved by continous analysis of the phase transition process monitored via measuring the suitable physical property *P*. The problem of extracting thermodynamic information from the property *P*, where observed data are linear integral transforms of the quantity to be estimated, is solved as a Fredholm integral equation with a convoluted kernel of the type that occurs in transformation kinetics. The result of the analysis of transformation in a metastable system—continuous probability density function of transformation rates—is shown to provide otherwise inaccessible unique information about thermodynamic processes, namely, the dependence of activation energies on temperatures. This information is especially important with respect to the complexity of the structure which is known to influence in an important manner the kinetics of transformation processes. The approach has been tested on experimental data of model material (glassy Fe-Co-B) representing a complex metastable structure. The notion of microprocess distributions spatially correlated with the cluster structure of the amorphous state is generalized and discussed from the viewpoint of dynamic and spatial heterogeneities in complex systems.

DOI: 10.1103/PhysRevB.64.184202 PACS number(s): 61.20.Lc, 61.43.Dq, 64.60.My, 64.60.Qb

I. INTRODUCTION

A typical feature of modern materials with complex structure such as metallic glasses or glassy polymers is their metastable state. Knowledge about the processes controlling thermal and time stability and the rate of transition from metastable to a more stable (crystalline) state provides vital information for detailed determination of thermodynamical processes and for identification of microstructural processes taking place during phase transition and structural changes in general.

Until now the evaluation of the mechanism of these processes has usually consisted of the determination of a single value of the activation energy or, in rare cases, of the spectrum of activation energies with an *a priori* prescribed distribution, using a proper kinetic or rate theory. The results obtained so far indicate that in general the processes controlling transformation in metastable systems are neither simple nor unique; rather, they suggest a distribution reflecting the fundamental physical and thermodynamical properties of these complex structures and the special preparation procedures which can by no means be sufficiently described by classical calculations. The relationship between the thermodynamic state of a complex system (e.g., metallic glass, etc.) and the role of microstructural processes controlling transformation rates is not clear, especially with respect to the metastability of the initial amorphous state. It is therefore very desirable to provide a model-free distribution of process rates and eventually of activation energies from experimental data, which can then be more reliably coupled to theoretical calculations and objectively interpreted.

Theoretical calculation of transformation rate coefficients is a discipline of nonlinear science important for different fields of physics, chemistry, engineering, and biology. There are many areas which have contributed to the rate theory; for a complete enumeration and review see Ref. 1. Among these are, e.g., electrical transport, tunneling, including quantum tunneling effects, and especially diffusion processes in solids and in amorphous and disordered materials.[2] A detailed comparison of experimental data with theoretical models of reaction rates, especially with thermally activated rates, is rather difficult because in rate measurements the detailed rate behavior is naturally more difficult to extract from measured transformation data. The analysis of experimental results of transformation rates becomes therefore the most important area for further theoretical considerations related to the nature of the metastable state and the corresponding concepts of the reaction rate theory.

In recent years there have been a number of investigations dealing with the transition from the metastable state in amorphous alloys using various models for the interpretation of the measured data. Among these are, e.g., adapted models developed originally for transformations in polycrystalline solids or rather complicated single-atom diffusion models, which suppose concentration gradients being established also in the amorphous phase with proceeding transformation.[3] The assumption about the concentration gradient, however, was not verified in the majority of cases.[4] In other instances, the selected fundamental parameters for rates of nucleation and growth are input, usually as unwarranted constants, into fitting models; for details see Ref. 5. Many other experimental results indicate complications in using classical transformation theory,[6] especially with respect to the anomalous temperature dependence of the Arrhenius factor in diffusion measurements.

In amorphous metastable metallic systems transformation processes (relaxation, nucleation, crystallization) are thermally activated and are usually approached through the notion of the activated state. The complexity of these systems induces the existence of multiple initial metastable states, leading in turn to complicated transformation rate behavior with multiple values of the escape energy on the path to a

more stable state. Selected cases of this phenomenon were treated by Primak[7] and Gibbs *et al.*[8] who assumed that the activation energies of the processes, which are available to contribute to the experimentally observed change in a property P in the course of the transformation process, are distributed over a continuous spectrum with predefined shape. In general case, monitoring of the change in property P during the transformation process can be used to study the kinetics and energetics of this process. It turns out that free volume, electrical resistivity, specific heat, etc., can be taken as the property P.

In the case of amorphous metallic systems the transformation to a less metastable (crystalline) state leads to the formation of one single, usually metastable crystalline phase and its subsequent transformation to a more stable state takes place in the crystalline state.[9] Such a transformation may be plausibly described by one single type of reaction without invoking the necessity for a concentration gradient and with the same particle morphology (with constant morphology parameter). This implies the same transformation micromechanism throughout the whole transformation stage and does not exclude different initial potentials which are reflected in different activation energies distributed over the entire assembly and lead to a distribution of reaction rates. Furthermore, it has been shown that a random potential ensemble of Arrhenius-type processes, as may be expected in amorphous matter, with suitable energy distribution leads to non-Arrhenius behavior of the process rates.[10] This makes analysis of the transformations in amorphous metastable systems even more complicated.

As a consequence it is supposed that the mechanism controlling the transformation rates is composed of a spectrum of weighted processes. These processes are probably spread over a wide interval of such thermodynamic parameters as activation energy E_a and frequency factor ν and involve structural units with varying sizes which enter into the transformation processes or free volumes between interacting structural units. In complex structures such as amorphous alloys the heterogeneity of the local atomic enviroment[11] is expected to generate distributions of different thermodynamic processes.

From a continuous analysis of the time dependence of the experimentally monitored property $P(t)$ we shall determine in a general, model-independent manner the number and type of individual mechanisms and also the probability of occurrence of these mechanisms in transformation process from amorphous to crystalline structure. We shall determine the temperature dependence of the activation energies and evaluate the importance of this effect for thermally activated transformations such as appearing in metallic glassses. We shall test the developed approach on experimental isothermal data from the transformation of real amorphous Fe-Co-B glass.

II. DISTRIBUTIONS OF PROCESSES

In the conventional approach to the analysis of transformations from metastable state to a more stable one, the time dependence of selected experimental property $P(t)$ reflecting the proceeding transformation of structure is converted to the fraction of transformed volume (degree of crystallinity) as a function of time, $x(t)$. The function $x(t)$ may be described by the usual Johnson-Mehl-Avrami equation[12]

$$x(t)=1-\exp[-(\lambda t)^n]. \tag{1}$$

Here

$$\lambda=\lambda_0 \exp(-E_a/RT), \tag{2}$$

with E_a being the activation energy of the rate λ of the process controlling the transformation, λ_0 is the preexponential factor closely related to the frequency factor ν, and n is the Avrami parameter reflecting the mechanism of nucleation and growth.[13]

In the case of a single process of the Arrhenius type characterized by a single value of λ at fixed T, the activation energy E_a and the Avrami parameter n should be constant throughout the whole reaction and temperature independent.

The usual formulas for calculating E_a and n at a fixed value of x for different T are based on the determination of the slope of the logarithms of time-to-transition or rate-of-change values versus the inverse temperature and of the double-logarithmic dependence of $1/(1-x)$ versus logarithm of time, respectively.[14]

If the entire process of transformation is controlled by several processes which might have different rates, the function $x(t)$ can be represented as a weighted sum of these processes,

$$x(t)=1-\sum_{i=1}^{N} \alpha(\lambda_i)\exp[-(\lambda_i t)^n], \tag{3}$$

where N is the number of such processes, λ_i is the rate of the ith process respecting Eq. (2), and $\alpha(\lambda_i)$ is the normalized weight of the ith process, the normalization condition being

$$\sum_{i=1}^{N} \alpha(\lambda_i)=1. \tag{4}$$

In complex materials such as metallic glasses the existing local heterogeneity of the atomic ordering is expected to generate distribution of processes, yet without influencing the mechanism of the transformation, leaving the Avrami parameter n constant. A finite sum of few discrete processes may generally be quite inadequate to represent the complex system. Assuming a continuous distribution of processes controlling the transformation, Eq. (3) takes the form of integral

$$x(t)=1-\int_0^{\infty} \alpha(\lambda)\exp[-(\lambda t)^n]d\lambda \tag{5}$$

and the normalization condition is

$$\int_0^{\infty} \alpha(\lambda)d\lambda=1, \tag{6}$$

where for a continuous distribution of processes, $\lambda \in (0,\infty)$, the quantity $\alpha(\lambda)$ represents the probability density of the transformation process having the rate λ. The fraction of

transformation processes (occurrence) with rates between λ and $\lambda + d\lambda$ is given by $\alpha(\lambda)d\lambda$.

A. Fredholm integral equation

From a mathematical point of view the above-described problem of transformations controlled by a distribution of processes belongs to the class of ill-posed problems[15] which may be expressed as Fredholm integral equations of the first kind. Equation (5) represented in this form is

$$x(t) = 1 - \int_0^\infty s(\lambda) K(\lambda, t) d\lambda, \tag{7}$$

where the form of the kernel $K(\lambda,t)$ is known, $K(\lambda,t) = \exp[-(\lambda t)^n]$. For an ideal case when $x(t)$, the time dependence of the fraction of transformed volume at a fixed temperature, can be directly determined, the solution $s(\lambda)$ equals the probability density function of the rates of processes, $s(\lambda) = \alpha(\lambda)$.

The analysis of experimental isothermal transformation data is further complicated by the fact that generally the time dependence $x(t)$ is obtained via measuring the selected property P using a convenient instrumentation which has its own resolution function $R_{instr}(t)$. The two functions $x(t)$ and $R_{instr}(t)$ are convoluted with each other in the course of measurement. Thus instead of $x(t)$ rather a function $y(t) = R_{instr}(t) * [1 - x(t)]$, which corresponds to the property $P(t)$ with values ranging from $P(t=0)$ to $P(t \to \infty)$ or from 1 to 0 after suitable rescaling, is experimentally obtained in realistic measurements,

$$y(t) = R_{instr}(t) * \int_0^\infty \alpha(\lambda) \exp[-(\lambda t)^n] d\lambda$$

$$= R_{instr}(t) * \int_0^\infty s(\lambda) K(\lambda, t) d\lambda, \tag{8}$$

where $*$ is the operator of convolution.

The determination of $R_{instr}(t)$ can be avoided by measuring a transformation curve $x_r(t)$ of a reference material transforming in the reaction of the first order, $n=1$, with a single known value of the transformation rate λ_r and the known weight of the process α_r,

$$x_r(t) = 1 - \alpha_r \exp(-\lambda_r t), \tag{9}$$

which would be obtained under ideal measuring conditions, the value of $\alpha_r = 1$ for a suitable choice of the reference material. For a real case we measure the function $y_r(t)$ corresponding to the selected property of the reference material, giving

$$y_r(t) = R_{instr}(t) * [1 - x_r(t)]. \tag{10}$$

The functions $y(t)$ and $y_r(t)$ have the same resolution function $R_{instr}(t)$, being measured by the same apparatus under the same conditions, which is used in solving Eq. (8). Convolution of Eq. (8) with $1 - x_r(t)$ from Eq. (9) eliminates R_{instr},

$$[1 - x_r(t)] * y(t) = y_r(t) * [1 - x(t)]. \tag{11}$$

Putting $Z(t) = 1 - x(t)$ and $Z_r(t) = 1 - x_r(t)$ and solving for $y(t)$ by using the Laplace transform of the convolution product we obtain

$$y(p) = y_r(p) Z(p) \frac{1}{Z_r(p)}, \tag{12}$$

where

$$Z_r(p) = \frac{1}{p} - x_r(p) = \alpha_r \frac{1}{p + \lambda_r}. \tag{13}$$

Then

$$y(p) = A\, y_r(p) Z(p) (p + \lambda_r), \tag{14}$$

where $A = 1/\alpha_r$. Using the rules about the inverse Laplace transformations of functions and their derivatives of original we can write

$$y(p) = A[y_r(p) p\, Z(p) + \lambda_r y_r(p) Z(p) + y_r(p) Z(0) - y_r(p) Z(0)] \tag{15}$$

and after regrouping

$$y(p) = A\{y_r(p)[p\, Z(p) - Z(0)] + \lambda_r y_r(p) Z(p) + y_r(p) Z(0)\}. \tag{16}$$

The inverse Laplace transformation yields

$$y(t) = A[y_r(t) * Z'(t) + y_r(t) * Z(t) \lambda_r + y_r(t) * Z(0)\, \delta(t)]. \tag{17}$$

Substituting for $Z(0) = \int_0^\infty \alpha\, d\lambda$ and $Z'(t) = -\int_0^\infty \alpha\, n\, \lambda^n t^{n-1} \exp[-(\lambda t)^n] d\lambda$ we obtain

$$y(t) = A \int_0^\infty \alpha(\lambda) (y_r(t) + y_r(t) * \{\lambda_r \exp[-(\lambda t)^n] - n\, \lambda^n t^{n-1} \exp[-(\lambda t)^n]\}) d\lambda. \tag{18}$$

Assigning the kernel

$$K(\lambda, t) = A (y_r(t) + y_r(t) * \{\lambda_r \exp[-(\lambda t)^n] - n\, \lambda^n t^{n-1} \exp[-(\lambda t)^n]\}) \tag{19}$$

and performing suitable numerical integration to receive the convolution of $y_r(t)$ with the expression $(\lambda_r - n\, \lambda^n t^{n-1}) \exp[-(\lambda t)^n]$, the sought solution $s(\lambda) = \alpha(\lambda)$ of the Fredholm integral equation (18), identical to the solution of Eqs. (7) and (8), is obtained.

The conversion of the solution to other representations requires a transformation of the integration variable respecting the normalization condition, Eq. (6), because different probability density functions are not invariant against variable transformation. As λ varies usually over several decades, it is often suitable to represent the rate probability density function with respect to $\ln \lambda$. The occurrence of transformation processes with rates between $\ln \lambda$ and $\ln \lambda + d \ln \lambda$ is $\lambda \alpha(\lambda)\, d \ln \lambda$. Therefore, the rate probability density function normalized against $\ln \lambda$ is $\mathrm{PDF}(\ln \lambda) = \lambda \alpha(\lambda)$.

B. Application to real transformation processes

In order to solve the system of the above Fredholm linear integral equations by a numerical method we employed a constrained regularized least-squares method with options for peak constraints and linear equality and inequality constraints. A similar problem has been solved by Provencher[16] and modified by Gregory and Zhu.[17] Their program, known under the name CONTIN, is suitable for various physical problems which are described by equations corresponding to the ill-posed problems of the first order, $n=1$.

For our purposes we have developed a highly stable FORTRAN algorithm capable of processing noisy input data. The program uses a convoluted kernel containing higher-order exponentials, $n \geqslant 1$, of the type which occurs in the analysis of structure transformation data. The program performs the deconvolution and inverse Laplace transformation in a single step. The choice of the solution from the deconvolution is based on the principle of parsimony, i.e., the smoothest solution consistent with the experimental data and prior knowledge. The program employs a regularizer in the form

$$S = A_S^2 \int_{\lambda_{min}}^{\lambda_{max}} [s''(\lambda)]^2 d\lambda, \tag{20}$$

where A_S controls the size of the regularizer and thus the parsimony of the solution. The solution is computed in several hundred (typically 200) grid points over a suitably spaced interval $\langle \lambda_{min}, \lambda_{max} \rangle$ and provides a continuous transformation rate probability density function PDF(λ). The algorithm reflects also specific conditions given by the choice of electrical resistivity as the property P.

The determination of a known reference function $y_r(t)$ introduced in order to avoid direct estimation of the instrument function has been performed by measuring a simple experimental decay curve (of the first order) with known parameters. The instrument resolution function $R_{instr}(t)$ was simulated by the Gaussian function

$$R_{instr}(t) = \frac{1}{\sigma\sqrt{\pi}} \exp[-(t/\sigma)^2], \tag{21}$$

with a full width at half maximum (FWHM) $= 2\sigma\sqrt{\ln 2}$ where σ was chosen to provide a narrow Gaussian corresponding to the integration times of the measuring equipment, typically less than 1 s. The known functions $x_r(t)$, e.g., discharging of a capacitance standard, have been used to test the validity of the estimation of R_{instr} and to provide the $y_r(t)$ data as well as the parameters λ_r and α_r suitable to be used in the deconvolution algorithm.

We have analyzed the experimental data of the amorphous alloy $Fe_{64}Co_{21}B_{15}$, which is a model complex system in a metastable state undergoing a transformation to a more stable, crystalline structure. The evolution of electrical resistivity $R(t,T)$ in the course of structural transformations usually reflects well changes taking place in the structure. In isothermal conditions the electrical resistivity $R(t)$ decreases in the course of the transition in two distinct steps which correspond to the two crystallization reactions, as shown in Fig. 1. Complete information on the crystallization products is given in detail in Ref. 18.

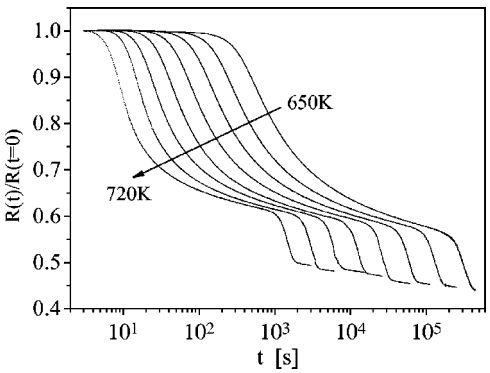

FIG. 1. The experimental time dependences of the isothermal electrical resistivity $R(t,T)$, selected as the property P, at constant annealing temperature 650, 660, 670, 680, 690, 700, 710, 720 K for amorphous alloy $Fe_{64}Co_{21}B_{15}$.

The transformation process of metastable structure starts at the very moment the sample is exposed to the selected temperature; thus, it is necessary to employ equipment capable of measuring and recording the transformation data as close to $t=0$ as possible and at stable enough temperature since the beginning of measurement. In our case the measurements start 3 s after the insertion of the sample in the measuring apparatus and data readings are taken in equidistant logarithmic time intervals to ensure a sufficient number of data points (several thousands) for each isotherm analyzed, yet with high enough accuracy (± 1 ppm). The measurements span over several time decades, typically from 3 to 10^6 s, allowing one to access a wide interval of transformation rates and crystallinity content from zero to complete crystallization over a range of temperatures of ~ 100 K. The transition from resistivity-time to $y(t)$ dependences has been performed using the serial model of electrical resistivity.[19] Its validity has been checked by the determination of the fraction of transformed volume using structure analysis methods (transmission electron microscopy and x-ray diffraction analysis) (Ref. 18) to the degree of accuracy of these methods, which, however, is of the order of a few percent. Except for an eventual systematic error due to application of the serial model of electrical resistivity, the accuracy of the measurement of resistivity, time, and temperature and the temperature stability gives the accuracy of the determination of activation energies better than $\sim 1\%$.

The measured electrical resistivity-time dependences have been analyzed by the developed algorithm to obtain the transformation rate probability density functions for all selected annealing temperatures. The results, i.e., the solution of ill-posed problems from Eq. (8), are presented in Fig. 2. The distributions were calculated for different exponents n in Eq. (8); the best results were obtained for the value of the Avrami parameter $n=4$, corresponding to intense nucleation and three-dimensional grain growth in both steps of the transformation process.

C. Distribution of activation energies

The classical analysis makes use of the positions of several maxima in PDF($\ln\lambda$)$=\lambda\,\alpha(\lambda)$ which may be assumed to

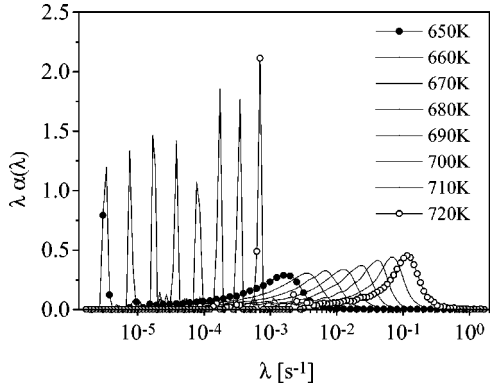

FIG. 2. The normalized probability density functions of rates of the transformation process, $\mathrm{PDF}(\ln\lambda)=\lambda\,\alpha(\lambda)$, vs the transformation rate λ at eight annealing temperatures for the amorphous alloy $Fe_{64}Co_{21}B_{15}$. The distributions are normalized against $\ln\lambda$. Solid curves are drawn through grid points merely for clarity.

correspond to typical transformation rates for different processes controlling the transformation. Selecting the rates λ for these processes at different temperatures and plotting them in an Arrhenius plot one obtains the values of the activation energies E_a and the corresponding preexponential factors λ_0 from Eq. (2). The plot with values of the parameters E_a and λ_0 for both reaction steps is given in Fig. 3. It can be seen that the plots of $\ln\lambda(1/T)$ exhibit practically no deviation from linearity even for a rather broad span of annealing temperatures.

The distribution of processes as a function of their activation energies, $\mathrm{PDF}(E)$, can be obtained by transforming the process rates $\lambda(T)$ into activation energies E by means of Eq. (2) and by recalculating $\mathrm{PDF}(\ln\lambda)$ into $\mathrm{PDF}(E)$ using the normalization condition from Eq. (6) in the form

$$\int_0^\infty \mathrm{PDF}(E)\,dE=\int_{-\infty}^{\infty}\mathrm{PDF}(\ln\lambda)\,d\ln\lambda=1. \tag{22}$$

Expressing

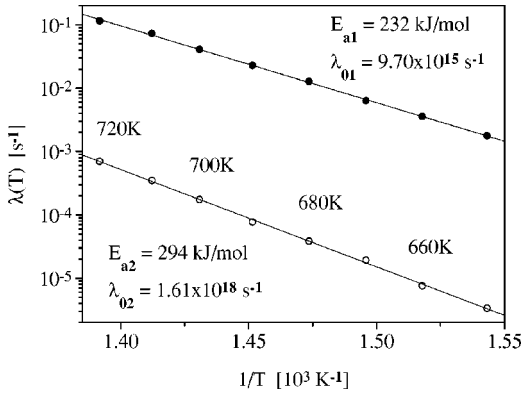

FIG. 3. Determination of the values of activation energies and preexponential factors for the two crystallization steps calculated using Eq. (2) from the peak positions of the transformation rate probability density functions shown in Fig. 2.

$$d\ln\lambda=\left(\frac{\partial\ln\lambda_0}{\partial E}-\frac{1}{RT}\right)dE$$

from differentiation of Eq. (2) we obtain

$$dE=\frac{1}{\dfrac{\partial\ln\lambda_0}{\partial E}-\dfrac{1}{RT}}\,d\ln\lambda.$$

For $E=0$ and $E=\infty$ the corresponding rates are λ_0 and 0, respectively. Putting

$$L=\frac{\partial\ln\lambda_0}{\partial E}$$

we obtain

$$\int_\infty^{\ln\lambda_0}\frac{\mathrm{PDF}(E(\ln\lambda))}{L-\dfrac{1}{RT}}\,d\ln\lambda=1.$$

The actual rates to be used as integration limits instead of λ_0 and 0 are λ_{max} and λ_{min}, respectively; therefore,

$$\int_{\ln\lambda_{\min}}^{\ln\lambda_{\max}}\frac{\mathrm{PDF}(E(\ln\lambda))}{\dfrac{1}{RT}-L}\,d\ln\lambda=1, \tag{23}$$

from which follows

$$\mathrm{PDF}(E)=\left(\frac{1}{RT}-L\right)\lambda\,\mathrm{PDF}(\lambda)=\left(\frac{1}{RT}-L\right)\mathrm{PDF}(\ln\lambda). \tag{24}$$

For themodynamically simple cases where the preexponential factor λ_0 is a constant independent on temperature and activation energy, the term $L=\partial\ln\lambda_0/\partial E=0$ and the transformation of the $\mathrm{PDF}(\ln\lambda)$ into $\mathrm{PDF}(E)$ takes the simple form

$$\mathrm{PDF}(E)=\frac{1}{RT}\lambda\,\mathrm{PDF}(\lambda)=\frac{1}{RT}\mathrm{PDF}(\ln\lambda).$$

In processes where a real dependence of the activation energy on temperature, $E=E(T)$, can be expected or where a formal interdependence between the activation energy E and preexponential factor λ_0 can be expected, $\lambda_0=\lambda_0(E)$, indicating a deviation of Eq. (2) from the ideal Arrhenius case, the quantity L shall be nonzero. In such cases the division of the $\mathrm{PDF}(\ln\lambda)$ dependences for different temperatures by RT will not yield a single curve and $L=L(E)$ has to be evaluated. The significance of this dependence and its importance for the interpretation of results shall be analyzed later.

Using the above relation, Eq. (24), for every annealing temperature T, the entire rate distribution curves ought to transform into a single temperature-indepenent activation energy distribution. The main problem in the computation has been the criterion for the construction of a matrix of times which correspond to a specific amount of transformed matter—degree of crystallinity—with a suitable correspon-

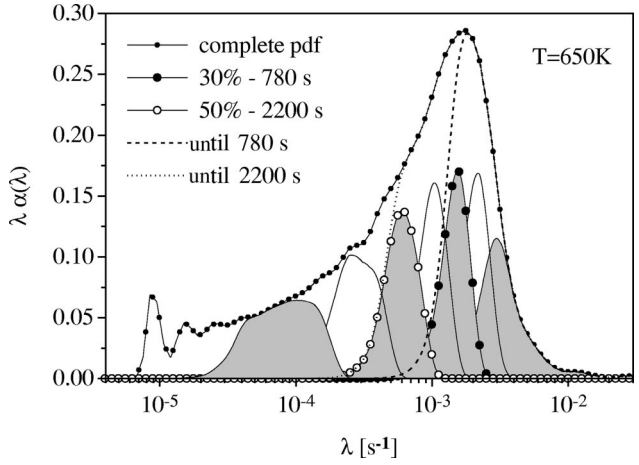

FIG. 4. Subdistributions of the processes from the overall transformation rate probability density function at selected annealing temperature 650 K active at specific times $t=360$, 540, 780, 1200, 2200, 5600, 30 000 s corresponding to the ''fractions of the transformed volume'' $x=10\%$, 20%, 30%, 40%, 50%, 60%, 70%, respectively (thin lines, shaded areas drawn for 10%, 30%, 50%, and 70%), with regard to the resistivity change from 0 to 76% for the first crystallization stage. The enveloping curve (thick line with small dots) represents the entire probability density function of transformation rates of crystallization process from amorphous to fully crystalline state. Dashed and dotted lines represent those processes which were annealed out until the selected times.

dence to transformation rates λ at each temperature which would justify the use of Eq. (2). At each of these times only a certain part of the distribution of processes is active in time interval from t to $t+dt$. Until this time t a certain part of the whole distribution of processes has already taken place, producing the corresponding crystallinity, i.e., has been ''annealed out,'' while the remaining part of the distribution is still awaiting ''activation.'' The distribution of processes annealed out until time t, $P_{anneal}(t,T)$, is given by the subintegral function in Eq. (5) expressed in $\ln\lambda$ scale convenient for the calculation of the activation energy distribution as

$$P_{anneal}(t,T)=\lambda\alpha(\lambda)\{1-\exp[-(\lambda t)^n]\}. \qquad (25)$$

The ''running,'' or active, processes at time t are given roughly by the difference of processes annealed out between the time t and $t+\Delta t$, so

$$P_{active}=\lim_{\Delta t\to 0}\frac{P_{anneal}(t+\Delta t)-P_{anneal}(t)}{\Delta t},$$

or, more exactly, as

$$P_{active}(t,T)=\frac{\partial P}{\partial t}dt=\lambda\alpha(\lambda)n(\lambda t)^n\exp[-(\lambda t)^n]d\ln t, \qquad (26)$$

where the quantity $P_{active}(t,T)$ represents the portion of processes active between $\ln t$ and $\ln t+d\ln t$. The situation is depicted in Fig. 4 where the dashed and dotted lines represent the subdistributions annealed out until the selected times and the lines and shaded areas represent the subdistributions

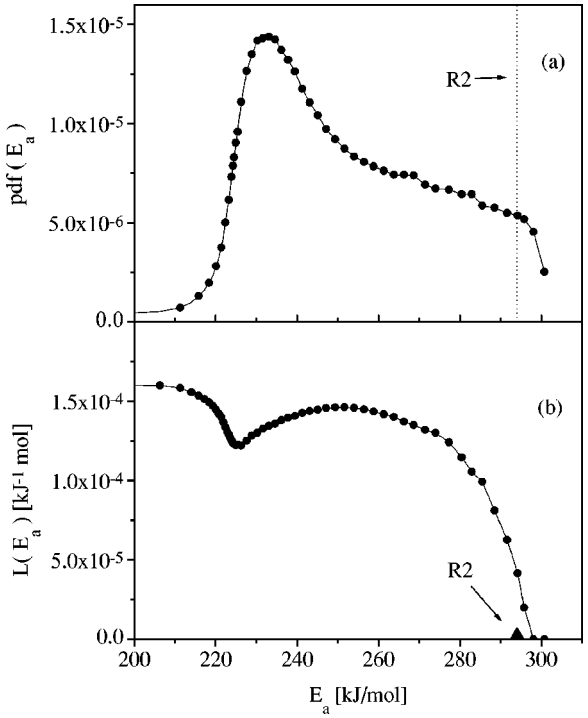

FIG. 5. (a) Probability density function of activation energies, PDF(E_a) vs E_a, determined by the complex analysis for both crystallization stages at eight annealing temperatures. Values of activation energies and preexponential factors were calculated from the peak positions and peak values of the subdistributions of active processes. The dotted line indicates the position of the very narrow distribution obtained for the second crystallization stage. (b) The dependence of the quantity $L=\partial\ln\lambda_0/\partial E$ on activation energy E_a for both crystallization stages. The value of L for the second stage (solid triangle) is indicated by the arrow.

of active processes. It is to be noted that the window in which the processes are active for the selected time t is quite narrow.

For each subdistribution at selected time t the ith moment has been calculated by

$$M_i=\int_{\ln\lambda_{\min}}^{\ln\lambda_{\max}}\lambda^{i+1}P_{active}(t,T)d\ln\lambda.$$

The average value $\langle\lambda\rangle$ of the subdistribution is given by M_0/M_{-1}. In this manner both PDF($\ln\lambda$) and $\langle\lambda\rangle$ for processes active in time t are unambiguously assigned to the selected time corresponding to the chosen fraction of transformed volume at each annealing temperature. Applying Eq. (2) the process rates can be transformed to the scale of activation energies, providing the values of λ_0 and E_a for different fractions of transformed volume. Then, using Eq. (24) for all annealing temperatures, PDF($\ln\lambda$) at these values of λ can be converted to PDF(E) using the values of L computed by a suitable minimalization procedure. The results of this procedure are shown in Fig. 5. It is to be understood that the activation energies obtained here are of the Arrhenius type from Eq. (2), i.e., correspond to the value $E_a\neq E_a(T)$ which comes from the slope of the plot of $\ln\langle\lambda(T)\rangle$ vs $1/T$.

D. Significance of the quantity *L*

As shown in Fig. 5(b), the values of L are nonzero and not constant over a broad interval of E_a. Let us, therefore, rewrite more realistically Eq. (2), including the above considerations, in logarithmic form as

$$\ln \lambda = \ln \lambda_{00} - \frac{E(T)}{RT}, \tag{27}$$

where the true preexponential factor λ_{00} used instead of λ_0 from Eq. (2) should be a constant and $E(T)$ represents the temperature dependence of activation energy. Let us approximate the dependence $E(T)$ in the vicinity of a certain temperature T_0 lying within the interval of selected annealing temperatures by the first two terms of the Taylor series in the form

$$E(T) = E(T_0) + E'(T - T_0), \tag{28}$$

where $E(T_0) = E_0$ is the value of activation energy E in T_0 and $E' = dE/dT|_{T_0}$. Substituting for $E(T)$ we can express Eq. (27) as

$$\ln \lambda = \ln \lambda_{00} - \frac{E'}{R} - \frac{1}{RT}(E_0 - E'T_0). \tag{29}$$

By comparison with Eq. (2) we see that

$$\ln \lambda_0 = \ln \lambda_{00} - \frac{E'}{R} \tag{30}$$

and

$$E_a = E_0 - E'T_0. \tag{31}$$

Then, repeating the procedure from Eq. (22),

$$\frac{d \ln \lambda}{dE_a} = -\frac{1}{R}\frac{dE'}{dE_a} - \frac{1}{RT}, \tag{32}$$

from which it follows that

$$L(E_a) = -\frac{1}{R}\frac{dE'(E_a)}{dE_a}. \tag{33}$$

The dependence $L(E_a)$ on E_a is already determined, so Eq. (33) may be considered as a differential equation which can be solved by numerical integration to give $E'(E_a)$, using the fact that the activation energy E_a is temperature independent for $L = 0$; therefore, $E'(E_{a,L=0}) = 0$. This is a restatement of the fact that E' represents the temperature dependence of E around T_0. Thus

$$E'(E_a) = R \int_{E_a}^{E_{a,L=0}} L(E_a) dE_a. \tag{34}$$

In order to obtain the distribution $\mathrm{PDF}(E_0)$ from $\mathrm{PDF}(E_a)$ [shown in Fig. 5(a)] we again used the normalization condition and variable transform from E_a to E_0. From Eqs. (31) and (33) we obtain $dE_0/dE_a = 1 - RT_0L(E_a)$ and

$$\mathrm{PDF}(E_0) = \frac{1}{1 - RT_0L(E_a)}\mathrm{PDF}(E_a). \tag{35}$$

The $\mathrm{PDF}(E_0)$ dependence represents the distribution of processes in true activation energy at a fixed temperature T_0. In order to be able to compute such a distribution for other temperatures around T_0, we have to repeat the process described above, transforming from E_0 to true $E(T)$. Using a one-to-one correspondence between E_a and E_0 we can write $L = L(E_0)$ to obtain

$$\mathrm{PDF}(E) = \frac{1 - RT_0L(E_0)}{1 - RTL(E_0)}\mathrm{PDF}(E_0). \tag{36}$$

In this way the distributions $\mathrm{PDF}(E(T))$ can be obtained for annealing temperatures from low values up to a limiting value of $T_{max} \leqslant 1/RL_{max}$. As follows from Eq. (24), the maximum value of L, L_{max}, should not exceed the value $1/RT_{anneal\ max}$, where $T_{anneal\ max}$ is the highest annealing temperature used, which was 720 K in our case; Fig. 5(b) shows that the maximum value of L is in fact $\sim 1.64 \times 10^{-4}$ $\mathrm{kJ^{-1}\,mol}$, below this value. Therefore, $T_{max} \leqslant 730$ K.

III. RESULTS

This section shows the results of the application of a continuous distribution analysis to the transformation from the amorphous metastable state to the crystalline state in $Fe_{64}Co_{21}B_{15}$ metallic glass. The distribution of activation energies, $\mathrm{PDF}(E_a)$, Fig. 5(a), starts smoothly from about 200 kJ/mol and attains a maximum at 232 kJ/mol, a value which is in excellent agreement with the results for E_{a1} from classical Arrhenius analysis in Fig. 3. The E_a distribution of the first crystallization reaction spreads further in a generally decreasing manner up to about 300 kJ/mol where it vanishes. The distribution for the second crystallization reaction is very narrow, practically corresponding to one single activation energy of about 295 kJ/mol, and yields $L = 0$.

The observed ratio of the changes of electrical resistivity with crystallization is 76% vs 24% for the first and second reactions, respectively. Detailed structure analysis, however, indicates that after the first crystallization about half of the entire sample volume remains amorphous. This ratio influences fortunately only the mutual ratio between the $\mathrm{PDF}(E_a)$ for the two crystallization stages, influencing in no way the shapes of the distributions.

A very important factor for obtaining the distribution of activation energies has been the determination of L for each value of activation energy taking part in the transformation process. The dependence $L = L(E_a)$ is shown in Fig. 5(b). It can be seen that the values of L decrease from a broad plateau towards zero close to the end of the first stage of crystallization. With respect to the origin of this quantity it can be supposed that the portion of activation energies dependent on temperature is exhausted with the proceeeding crystallization. Analysis of the second crystallization stage yields L equal strictly to zero; thus, the activation energy for this stage is temperature independent.

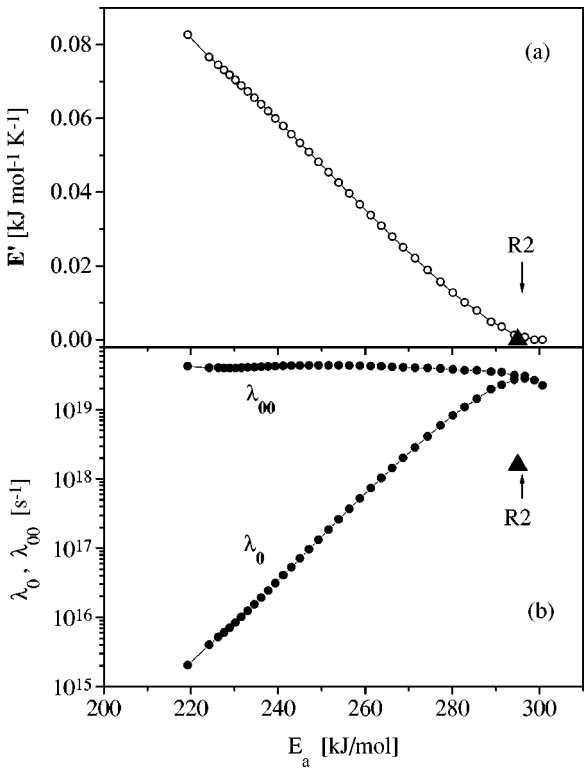

FIG. 6. (a) The dependence of E' on activation energy E_a. (b) The dependence of λ_0 and λ_{00} on activation energy E_a. Arrows indicate the corresponding values (solid triangles) for the second crystallization stage.

The dependence $E'(E_a)$ is shown in Fig. 6(a). Knowing $E'(E_a)$ we can immediately compute $\ln \lambda_{00}$ and E_0. Figure 6(b) shows the dependence of λ_{00} on E_a as well as the dependence of λ_0 from Eq. (2) on E_a for comparison. While λ_0 varies over more than five orders of magnitude, the value of λ_{00} is practically constant, confirming the assumption from Eq. (27). The plots of $E'(E_0)$ and PDF(E_0) are shown in Fig. 7. The influence of the temperature dependence of $E(T)$ on activation energy distribution, PDF$(E(T))$, for all eight annealing temperatures is shown in Fig. 8.

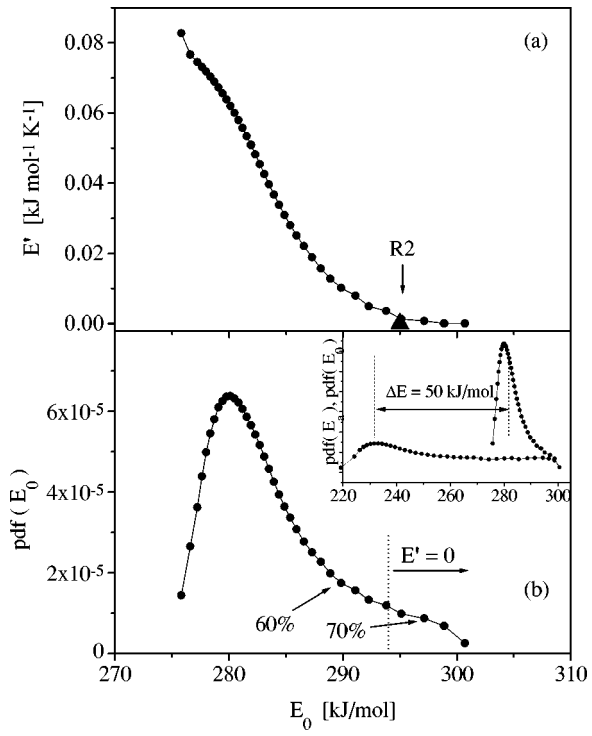

FIG. 7. (a) The dependence of $E'(E_0)$ on activation energy E_0. The solid triangle shows the corresponding value of E' for the second crystallization stage. (b) The probability density function of activation energies E_0, PDF(E_0). The value E' is zero for activation energies above the dotted line. Different ''fractions of the transformed volume'' close to the end of the first crystallization stage, which is 76% with regard to the resistivity change from 0 to 100%, are indicated by arrows. The inset in (b) shows the quantitative difference of 50 kJ/mol between PDF(E_a) and PDF(E_0) in the same scale.

IV. DISCUSSION

A. Cluster structure of metallic glasses

The results obtained on the selected investigated system, Fe-Co-B metallic glass, demonstrate the functioning of the approach developed in previous sections. It is clearly shown that by using this approach unique and until now inaccessible information on the transformation from amorphous state is obtained. The specific metastable system selected for testing has been chosen, besides others, also for the availability of transformation data on this system obtained by classical analyses[18] and thus for easy comparison of the progress using the continuous rate distribution analysis and the thermodynamic considerations above.

The initial state of metallic glass is metastable; the structure reflects the arrangement of constituent atoms as frozen in from the melt by the process of rapid quenching. Such a structure has to exhibit several specific features. To begin, the arrangement can be expected to copy the structure and the heterogeneities of the melt precursor. Further heterogeneities can arise from the dynamics of the uneven distribu-

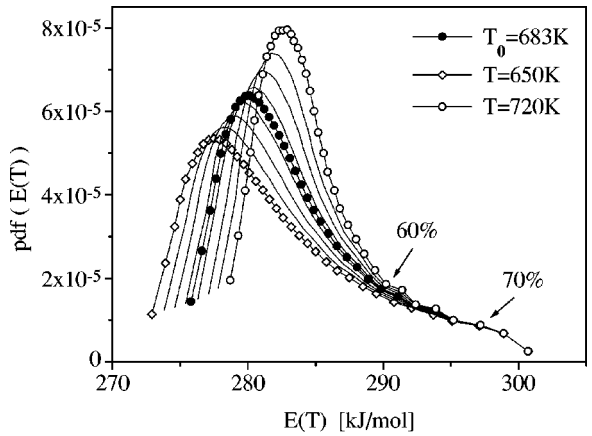

FIG. 8. The set of PDF$(E(T))$ for all eight annealing temperatures and for T_0, showing the influence of the temperature dependence of $E(T)$ on the activation energy distibutions. Arrows as in Fig. 7.

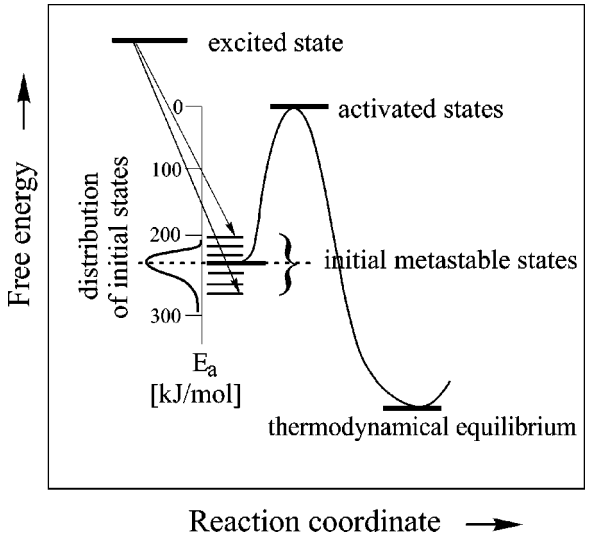

FIG. 9. Qualitative scheme showing the origin of the distributions of initial energetic states which lead to the distribution of thermodynamic processes controlling the transition from amorphous to a more stable crystalline state.

tion of temperatures in the course of quenching or from preferential local ordering between different types of atoms. The initial thermodynamic state of even the simplest amorphous system should thus be distributed over a range of possible local orderings and energetic states around a certain mean value specific for the material, which ought to be reproducible, reflecting the reproducibility of the rapid quenching process.

The thermodynamic heterogeneity on the scale of the local atomic environment in which transformation takes place is expected to generate the distribution of reaction rates. This genesis is caused at least by the distribution of activation energy levels corresponding to the distribution of initial energy levels with different density of occupation of these states given by the above reasons. The situation is schematically illustrated in Fig. 9 together with a possible distribution of initial states in activation energies.

Further reasons for such initial distributions of energetic states come from the inherent nature of the amorphous alloy given by the heterogeneity of the quenched-in structure of the melt. Besides structural and compositional heterogeneities on an atomic scale, experimental evidence in general suggests the possible formation of more complex, relatively stable, structural units—clusters—in the melt with chemical and partly also topological ordering which are preserved by rapid quenching. This adds another dimension to the complexity of the amorphous state due to the existence of such locally ordered, yet amorphous, structural units with different thermodynamic stability. It is highly probable that if such units are relatively stable, the transformation process shall include their transition to the crystalline state without a total rearrangement of atoms constituting the cluster by a process combining suitable collective motion across the interface with amorphous matrix and slight rearrangement of atoms to equilibrium conditions.

Such initial amorphous structure (and, consequently, initial energy distribution) can lead to enhanced temperature dependence of the transformation rates of processes compared to that given by Arrhenius-type relation valid for simple transitions involving the interaction or motion of single atoms. A more complex atomic envirnoment may induce an effective or apparent dependence of the activation energy on temperature or may lead to a temperature dependence of the transformation rates other than that given by Eq. (2). Such dependences have been suggested for processes in more complex polyatomic or molecular systems.[20–22] Another reason for the enhanced temperature dependence of transformation rates may lie in the fact that atomic jumps may influence the surrounding matrix and the thermodynamic states of other atoms therein or by enabling processes with thermodynamic parameters slightly differing from those of the ''parent'' process.[8] Activation of one process in an array of processes distributed in activation energies may change the resulting structure and the density of the remaining processes. All these factors lead to either a real or apparent dependence of the activation energy on temperature or to a commonly observed apparent dependence of the preexponential factor λ_0 on the activation energy.

It is quite striking to note that the true distribution of processes runs over a much narrower interval of activation energies than would be an estimate, if possible, from the classical approach using E_a. The end of the first reaction stage demonstrates very well the decrease of the temperature dependence of the active processes towards that described by Eq. (2); see Fig. 8. This is an indication that processes more complex in temperature dependence are more active in the earlier crystallization stages, i.e., in the presence of a large amount of amorphous matter (in abundance of the original amorphous structure). The interval of activation energies $E(T)$ is shifted to higher values by ~ 50 kJ/mol as compared to the peak position in the E_a distribution, Fig. 7. Such an effect has been frequently observed experimentally[6] and represents a typical discrepancy between measurements of, e.g., the self-diffusion coefficient in amorphous (complex) and polycrystalline structures.

In order to be able to check the quality of the information with the possibility to extrapolate towards lower temperatures, it is necessary to make yet one more variable transform from E to $\ln\lambda$. It can be shown that this transformation is quite straightforward and follows from Eq. (27). The comparison with the original PDF($\ln\lambda$) obtained from solution of the Fredholm integral equation by the deconvolution procedure (Fig. 2), as seen from Fig. 10, is excellent. Figure 11 demonstrates the capability of the prediction of the low-temperature behavior of the measured property P, electrical resistivity in our case, which is an important indication of the stability of the material. The dependence of $R(t)$ computed for low temperature (500 K) by the classical time-to-transition approach differs from the one computed via PDF(E) in time and shape, showing only a limited capability of the classical approach to deal with nonisokinetic behavior. For such cases the inaccuracy in the estimation of the thermodynamic stability of the system may be of the order of years, significant for potential technological applications.

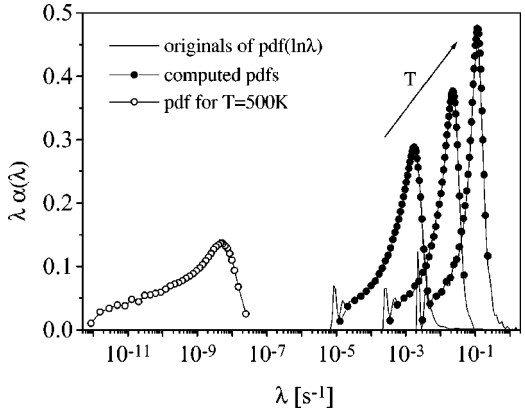

FIG. 10. Comparison of original distributions PDF($\ln\lambda$) $=\lambda\,\alpha(\lambda)$ from Fig. 2 (lines) for 650, 690, and 720 K with the dependences calculated from the curves in Fig. 8 transformed into $\ln\lambda$ representation (dots) showing excellent agreement with the original distributions. Extrapolation to low temperatures is shown by PDF($\ln\lambda$) calculated for 500 K; the shape of the distribution is markedly affected by the different temperature dependences of activation energies.

The dotted curve represents $R(t)$ for the same temperature, however using the classical aproach with a single value of E_a. The presentation of the distribution of the activation energy spectrum as a function of time is a complete representation of the formal kinetic behavior of a suitable property for most kinds of annealing programs. In this way it is also possible to deal with different types of processes with the same activation energy E, differing in λ_0, thus active in different times.

It has been shown, e.g.. in Ref. 13 that the entire activation energy, either E_0 or $E(T)$ in our notation, is a weighted sum of the activaton energies for nucleation and for growth. It is known that the activation energy for nucleation has an implicit dependence on temperature.[14] It would be worthwhile to consider again the phenomenological reasoning in Ref. 13 in view of the results on E_0 and its temperature derivative from Fig. 7. The quantity E' approaches zero for late stages of the first crystallization step. Let us suppose that the temperature dependence of $E(T)$ is generated by complicated process of formation of nuclei from the amorphous phase, as specified above (local heterogeneity, short-range ordering, or cluster structure leading, e.g., to a distribution of initial states, correlated motion of atoms, etc.). This may give rise to an activation energy of nucleation even more strongly dependent on T than in Ref. 12. The disappearance of the temperature dependence of the activation energy only towards the end of the first crystallization stage as well as detailed quantitative structure analysis[18] indicates a correct choice of the Avrami parameter (order of the reaction) $n=4$ corresponding to continuing nucleation almost until the end of this stage accompanied by three-dimensional growth.

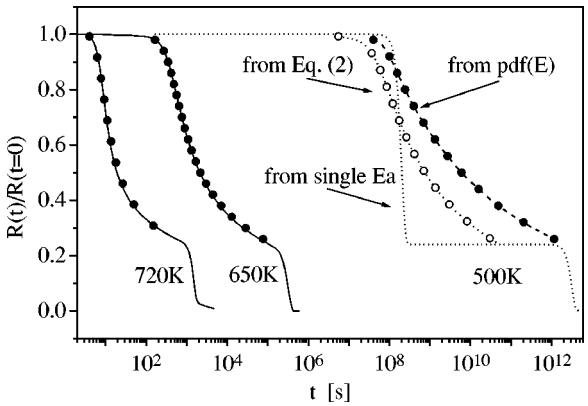

FIG. 11. Comparison of normalized experimental data of electrical resistivity for 650 and 720 K (solid lines) with the values computed using PDF(E) (dots). For illustration of the predictive capability of the complete PDF(E) representation, values computed for 500 K are shown for different models. Lines through points are drawn for clarity. Dotted line: simulation of $R(t)$ for 500 K using single values of activation energies taken from Fig. 3.

As noted briefly in the initial sections, Eqs. (1) and (2) are valid for ideal transformations characterized by a single process only. The addition of even one more process in the course of the transformation yields in most cases quite inaccurate results which are, at the best, only an average of the thermodynamic parameters (activation energy, preexponential factor) of the running processes. Exceptions may occur eventually when the processes are well separated in time and/or temperature. The values of the Avrami parameter obtained are not even rough estimates of the true mechanisms of transformation. Any distribution of processes with different activation energies, however simple, would lead to the dependences of the property $P(t)$ used to monitor the transformation, which would deviate from isokinetic behavior. The above-described approach easily allows the analysis of such curves using advantageously the notion of moments and subdistributions of processes.

The formulation of Eq. (3) or (5) is based on the assumption that the ith process, defined by its own λ_i, is predetermined to take place on several suitable larger-sized regions, ending in formation of final crystallinity produced by this type of process, $x_i(t\to\infty)$ where $x(t\to\infty)=\Sigma_i x_i(t\to\infty)=1$ and $x(t)=\Sigma_i x_i(t)$. Thus the transformation of amorphous structure to a more stable state takes place as a weighted sum of all possible subtransformations. The complexity and heterogeneity of the metastable structure on different size scales (short- and medium-range ordering of amorphous structure) make such an approach plausible. For the case of the model material used, glassy Fe-Co-B, this is supported also by the character of the second crystallization stage[18] where the remains of the amorphous phase representing about one-half of the entire volume transform monoenergetically by the same mechanism.

B. Spatial heterogenity in supercooled liquids and glasses

The considerations presented in the preceding subsection are based on more solidlike than liquidlike features of metallic glasses where the glass transition temperature T_g is seldom lower than the crystallization temperature; conversely, as the mobility of constituent structural units increases upon approaching the glass transition, rearrangements leading to a structure transformation take place.

The mechanism of formation of complex disordered metastable systems is similar for conventional metallic glasses, bulk metallic glasses, supercooled (glass-forming) molecular liquids, polymeric systems, and miscellaneous amorphous systems as biomolecules, proteins, colloids, etc. The liquid or melt is cooled below its melting point, and the dynamics slows dramatically due to cooling and even more dramatically in the proximity of the glass transition. Supercooled liquid falls out of equilibrium and exhibits behavior different from that expected for a homogeneous liquid—attaining a metastable state characterized by heterogeneous behavior, i.e., by varying dynamics in different regions lying close to each other. Whether this dynamics can be correlated with spatial heterogeneity is still an open question and a subject of investigation.[23]

While the origin of the spatial heterogenity of the dynamics in supercooled molecular liquids or polymer systems above the glass transition may be unclear, in the glassy state heterogenities are more plausible. The glassy system may be expected to behave more solidlike. The same can hold for supercooled liquids below a certain critical temperature, yet above T_g.[24] This picture is suggestive of a convenient potential energy landscape which in solidlike systems immediately provides a distribution of initial TD states (see Fig. 9). The same effect may be expected also from the fluctuations of local density or entropy related to local atomic or orientational ordering.[25] Another appealing approach which correlates, at least on mesoscopic scales, the distribution of dynamics with a spatial distribution of frustration-limited domains with preferred local packing was proposed in Ref. 26.

The answer should be related to the chemical identity of the glass formers and especially to their microstructure on atomic scales viewed from the point of existing interatomic or structurally correlated cluster bonding.[27] This effect may be different for supercooled molecular liquids and metallic glasses due to the nature of the constituent atoms: while in the former the size of ''molecules'' (high molecular weight) makes immediately plausible the notion of larger clusters or cooperatively rearranging regions,[28] the cluster structure of the latter is experimentally more difficult to evidence, especially due to the much smaller size of the expected locally ordered region. This point may also be of interest when treating the degree of fragility of glass formers and the origin of the glass-forming ability.[29,30]

It has to be noted that the vast majority of experiments treat heterogenity in dynamics; structural heterogenity is in general not unambiguously experimentally correlated with heterogenity in dynamics. This is mostly the case of supercooled molecular liquids,[31] although such evidence for bulk metallic glasses using the same method [small-angle neutron scattering (SANS)] exists.[32] Recently, evidence of cluster structure, i.e., structure heterogenity, and its stability at low and high temperatures in FeCoB was presented in Ref. 33. The difference in observability may reside again in the typical combination of atom species (metal and metalloid atoms in metallic glasses and covalently bonded molecular liquids).

Of the principal questions concerning the size, lifetime, dynamics, and origin of the spatial heterogenities[23,34] the last one seems to be the most crutial. The genesis of the heterogenities may have at least two causes. The first one, common to all mentioned amorphous systems and their supercooled liquid precursors, lies in the thermodynamics of formation of these systems, either by deep quench or by rapid solidification, leading to nonequilibrium, yet long-living states, enhanced further by the state from which the quenching was realized: a dynamically stable structure of complex liquids, possibly heterogeneous on atomic scales,[35] is prevented from equilibration, leading to quenched-in heterogeneities with spatial relaxation times increased by tens of orders of magnitude as the temperature decreases from above the melting point down to the glass transition. The second, thermodynamically easily acceptable cause is the existence of dynamically stable distributions of ''embryos'' in the undercooled heteroatomic liquids or melts on the path towards a more stable state (e.g., prior to eventual crystallization), yet without sufficient mobility to realize the transition). Especially in liquids with strong heteroatomic bonding where the regular solution and Becker's model of nucleation[12] cannot be applied, concentration fluctuations can act as additional, and thermodynamically important, sources of local heterogeneities.[36] Thus spatial and dynamic heterogeneities can tentatively be made analogous to the generally accepted picture of nucleation from a solid or liquid phase with dynamic (embryonic) component roughly corresponding to homogeneous nucleation and eventually also a static component analogous to a situation leading to heterogeneous or time-dependent nucleation. It seems that the degree of heterogeneity, spatial or dynamic, can range theoretically from fully heterogeneous to fully homogeneous extremes, as pointed out in Ref. 37. A suitable overall relaxation or correlation function which may be determined by a suitable experiment (equivalent to the physical property P used in our considerations in previous sections) should reflect this phenomenon through a dependence which is extrinsically nonexponential and is intrinsically composed of exponentials distributed through a corresponding probability density function. Its shape and temporal evolution should reflect the static and dynamic components considered in the previous paragraph. Examples of such behavior are the typical Kohlrausch-Williams-Watts stretched exponentials equation or Eq. (5). The formal similarity between the two equations is evident and the choice between the two depends on the physical phenomenon investigated; the approach presented in previous sections applies almost immediately to either of them. Very frequently the apparent (extrinsic) Kohlrausch exponent deviates from unity, especially in the cases of polymeric systems with higher molecular weight. A careful treatment, however, provides values of the intrinsic Kohlrausch exponent nearly equal to 1.[38] The differences between the two exponents are usually closely correlated with the complexity of the investigated systems; in the case of the crystallization of the model metallic glass treated above, this corresponds roughly to the deviation observed between the apparent Avrami parameter as determined from Eq. (1) and its constant value $n=4$.

The temperature dependence of average relaxation times (or of average transformation rates) is notoriously known to

exhibit deviations from the Arrhenius behavior.[39] Numerous theories based. e.g., on the free volume model, entropy model, etc., were developed and frequently reviewed.[29] Most of them, however, treat average quantities derived from temperature measurements of property P rather than the intrinsic relaxation functions (or microprocess rates). The use of the approach outlined in previous sections provides information on the temperature dependence of the true, or intrinsic, activation energies. The approach may prove to be a useful tool for the evaluation and interpretation of the temperature data of such quantities as viscosity and different relaxation effects of supercooled liquids or undercooled melts and even a contribution to the phenomenon of the breakdown of mode-coupling theory in complex systems with heterogeneous features.[24,40] One of the possible advantages would be an analysis of the behavior of the narrower spectra of heterogeneities (spatial or dynamic), allowing for more accurate theoretical considerations, especially when considering spatially distributed heterogeneities. The quantity E' as defined above is typically negative for microprocesses in supercooled liquids.[29] A more complicated dependence of $E'(T)$ may be expected as the glass transition is approached[34] and in the cases of crystallization from a supercooled liquid or amorphous state. In addition to the increase of activation energy of nucleation with temperature as predicted by classical theories,[12] heterogeneity or fluctuation-enhanced nucleation[36] may play an important role in $E(T)$ dependence per crystallization event. Thus an indication of the type of microprocesses active in relaxation or transformation processes in general (or deviations from theoretical predictions) can be obtained, depending on the sign of E', being mostly positive for nucleation-controlled processes and mostly negative for viscous-flow-controlled processes; single-atom processes or processes in regular solutions ought to exhibit $E' \sim 0$.

V. CONCLUSION

We have developed a progressive and accurate approach to the analysis of the isothermal time dependences of the property $P(t)$, selected to reflect the transformation process in complex structures. We have considered the set of transformation isotherms as an ill-posed problem and we have obtained a continuous distribution of transformation rates from solution of a system of Fredholm integral equations. The effect of measuring instrumentation needed to obtain the time dependence of the transformed volume fraction, $x(t)$, and experimental noise were eliminated by the use of the deconvolution procedure and inverse Laplace transformation. From rate distributions PDF(λ), using moment analysis and by introducing the notion of subdistributions of transformation processes active at selected times we obtained the distributions PDF(E) of the true activation energy E. The information about the effects of the temperature dependence of activation energies, $E(T)$, not accessible until now, was also obtained from isothermal measurements.

On the basis of these results [PDF(λ), PDF($E(T)$)] we are able to identify and predict the time-temperature regions of interest for transformation and explain many discrepancies in the interpretation of results, yet keeping a constant morphology parameter (the Avrami parameter n) throughout the entire transformation stage. The results allow us to consider each transformation stage as controlled by a single type of microprocess with identical mechanism (i.e., identical preexponential factors) yet coming from different initial energetic states, as witnessed by the obtained distribution of activation energies. As the processes take place in a viscous amorphous medium, their temperature dependence is more complex than the Arrhenius relation. The results provide the sign and magnitude of the deviation of process rates from Arrhenius behavior and allow us justify the choice of controlling mechanism (nucleation, growth, diffusion, viscous flow, etc.) without any need for prior postulation of the presence of these mechanisms and based only on fundamental thermodynamic presumptions and the nature of the amorphous state.

This approach requires no free thermodynamic parameters in the evaluation of process kinetics, yet leads to constant values of the preexponential factor and provides new values of activation energies consistent with independent measurements such as mass transport in diffusion experiments. It also provides a tool for explaining the previously observed discrepancies in the activation energies and effects on preexponential factors. Among these are, e.g., differences of several orders of magnitude between the theoretical values from rate theories and those determined experimentally by classical methods and the interdependence of the preexponential factor on apparent activation energy in a plausible manner.

Our approach represents also a contribution to the philosophy about the cluster structure of the amorphous state which is in accordance with recent microstructural observations, especially the notion of the transformation of amorphous clusters into a metastable crystalline phase. This transformation mechanism may be thought to take place by preservation of the local ordering of the cluster structure in the first crystalline phase formed in the transformation process via small motion of entire clusters and slight atomic rearrangement taking place upon crossing the interface. Careful use of the approach provides the possibility of obtaining information on early stages of the transformation (nucleation processes), their temperature dependence, and their influence on the transformation mechanism. From this viewpoint the concept of primary crystallization controlled by long-range diffusion, resulting from the use of a classical single-atom approach to transformation rates, in clustered amorphous media becomes quite inapplicable. Short-range ordering and cluster structure override the contribution from the motion of single atoms over (long) distance due to a small portion of ''free'' unclustered atoms in the matter.

ACKNOWLEDGMENTS

The authors express their thanks to the Grant Agency for Science of Slovakia and NATO Science for Peace for the support of this research (Grant Nos. 2/6064/99 and SfP-973649).

[1] P. Hänngi, P. Talkner, and M. Borkovec, Rev. Mod. Phys. **62**, 251 (1990).
[2] H. Kronmüller and W. Frank, Radiat. Eff. Defects Solids **108**, 81 (1989).
[3] D. Crespo, T. Pradell, M.T. Clavaguera-Mora, and N. Clavaguera, Phys. Rev. B **55**, 3435 (1997).
[4] K. Hono, D.H. Ping, M. Ohnuma, and H. Onodera, Acta Mater. **47**, 997 (1999).
[5] K.F. Kelton, K. Lakshmi Narayan, L.E. Levine, T.C. Cull, and C.S. Ray, J. Non-Cryst. Solids **204**, 13 (1996).
[6] H. Kronmüller, W. Frank, and A. Hörner, Mater. Sci. Eng., A **133**, 410 (1991).
[7] W. Primak, Phys. Rev. **100**, 1677 (1955).
[8] M.R. Gibbs, J.E. Evetts, and J.A. Leake, J. Mater. Sci. **18**, 278 (1983).
[9] P. Duhaj and P. Švec, Mater. Sci. Eng., A **226/228**, 245 (1997).
[10] T.A. Vilgis, J. Phys. C **21**, L299 (1988).
[11] J.D. Ayers, V.G. Harris, J.A. Sprague, W.T. Elam, and H.N. Jones, Acta Metall. **46**, 1861 (1998).
[12] J.W. Christian, *The Theory of Transformations in Metals and Alloys* (Pergamon Press, Oxford, 1975), Pt. I.
[13] M.V. Heimendahl and G. Kuglstatter, J. Mater. Sci. **16**, 2405 (1981).
[14] J. Burke, *The Kinetics of Phase Transformations in Metals* (Pergamon Press, Oxford, 1965).
[15] A.N. Tichonov and A.A. Samarskij, *Equations of Mathematical Physics* (Nauka, Moscow, 1951).
[16] S.W. Provencher, Comput. Phys. Commun. **27**, 229 (1982).
[17] R.B. Gregory and Y. Zhu, Nucl. Instrum. Methods Phys. Res. A **290**, 172 (1990).
[18] 2nd Year Progress Report, PECO Programme CIPA-CT93-0239, pp. 39–52 (1996).
[19] R. Landauer, J. Appl. Phys. **23**, 779 (1952).
[20] A.K. Doolittle, J. Appl. Phys. **22**, 1471 (1951).
[21] H.S. Chen, J. Non-Cryst. Solids **22**, 135 (1976).
[22] J.H. Gibbs and E.A. Di Marzio, J. Chem. Phys. **28**, 373 (1958).
[23] M.D. Ediger, Annu. Rev. Phys. Chem. **51**, 99 (2000).
[24] A.P. Sokolov, J. Non-Cryst. Solids **235-237**, 190 (1998).
[25] M.D. Ediger, J. Non-Cryst. Solids **235-237**, 10 (1998).
[26] D. Kivelson, S.A. Kivelson, X.L. Zhao, Z. Nussinov, and G. Tarjus, Physica A **219**, 27 (1995).
[27] M. Oguni, J. Non-Cryst. Solids **210**, 171 (1997).
[28] Y. Hiwatari and T. Muranaka, J. Non-Cryst. Solids **235-237**, 19 (1998).
[29] J.C. Dyre, J. Non-Cryst. Solids **235-237**, 142 (1998).
[30] C.A. Angell, Science **267**, 1924 (1995).
[31] R.L. Leheny, N. Menon, S.R. Nagel, D.L. Price, K. Suzuya, and P. Thiyagarajan, J. Chem. Phys. **105**, 7783 (1996).
[32] J.F. Löffler and W.L. Johnson, Mater. Sci. Eng., A **304-306**, 670 (2001).
[33] K. Krištiaková and P. Švec, Phys. Rev. B **64**, 014204 (2001).
[34] C.Y. Wang and M.D. Ediger, J. Chem. Phys. **112**, 6933 (2000).
[35] V. Sidorov, P. Popel, M. Calvo-Dahlborg, U. Dahlborg, and V. Manov, Mater. Sci. Eng., A **304-306**, 480 (2001).
[36] E. Cini, B. Vinet, and P.J. Desré, Philos. Mag. A **80**, 955 (2000).
[37] R. Böhmer, R.V. Chamberlin, G. Diezemann, B. Greil, A. Heuer, G. Hinze, S.C. Kuebler, R. Richert, B. Sciener, H. Silescu, H.W. Spiess, U. Tracht, and M. Wilhelm, J. Non-Cryst. Solids **235-237**, 1 (1998).
[38] H. Wendt and R. Richert, Phys. Rev. E **61**, 1722 (2000).
[39] G. Tarjus, D. Kivelson, and P. Viot, J. Phys.: Condens. Matter **12**, 6497 (2000).
[40] C. Donati, S.C. Glotzer, P.H. Poole, W. Kob, and S.J. Plimpton, Phys. Rev. E **60**, 3107 (1999).